STRUCTURAL APPLICATIONS OF MECHANICAL ALLOYING

Proceedings of an
ASM International® Conference
Myrtle Beach, South Carolina
27–29 March 1990

Edited by
F. H. Froes and J. J. deBarbadillo

Published by
ASM International®
Materials Park, Ohio 44073

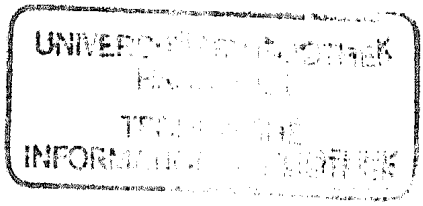

ASM International® is a Society whose mission is to gather, process and disseminate technical information. ASM fosters the understanding and application of engineered materials and their research, design, reliable manufacture, use and economic and social benefits. This is accomplished via a unique global information-sharing network of interaction among members in forums and meetings, education programs, and through publications and electronic media.

Library of Congress Catalog Card Number: 90-062191
ISBN: 0-87170-390-4
SAN: 204-7586

ASM International®
Materials Park, Ohio 44073

Printed in the United States of America

THE TRANSVERSE CREEP BEHAVIOUR OF MA 6000 IN TENSION AND COMPRESSION

Russell Timmins, Eduard Arzt
Max-Planck-Institut für Metallforschung
Institut für Werkstoffwissenschaft
Seestrasse 92,7000 Stuttgart 1
FRG

ABSTRACT

Poor transverse strength is a possible limitation for the widespread application of coarse-grained oxide dispersion strengthened (ODS) alloys at high temperatures. This work presents new tensile and compressive creep results, produced with continuous strain measurement, on MA 6000, which reveal the important micromechanisms responsible for the inferior high temperature performance under transverse loading. A model based on an interface reaction controlled diffusional creep mechanism is presented, which is the basis for a better understanding of the transverse creep behaviour of ODS alloys.

1.0 Introduction

Oxide dispersion strengthened (ODS) superalloys are promising materials for critical components operating at elevated temperatures. In particular these alloys, following controlled thermo-mechanical processing, possess excellent creep strength which is primarily due to a fine dispersion of inert oxide particles. The understanding of the creep deformation and fracture behaviour of ODS alloys has advanced considerably in recent years (for a review see Ref.1). A new constitutive equation (1,2) based on the thermally activated detachment of dislocations from inert dispersoids has led to a more consistent interpretation of the creep deformation behaviour in ODS alloys; in particular the high stress exponents and activation energies for creep, which are typical for ODS materials in general, are accounted for in a more natural way.

Efficient strengthening in nickel base ODS superalloys by inert dispersoids is achieved, however, only in combination with an elongated grain structure which suppresses excessive accumulation of creep fracture damage. This role of grain geometry in the creep deformation and fracture behaviour of ODS alloys has also received attention (3-7), but there still remains much debate over the detailed mechanisms involved. Furthermore, the presence of an elongated grain structure, which is a prerequisite for good high temperature creep strength, naturally leads to a far from optimum grain geometry in the transverse direction with a consequent degradation in creep behaviour. Since critical components are rarely subjected to uniaxial loading alone, it is essential to gain a better understanding of the transverse creep properties.

In this contribution emphasis is placed on the transverse creep behaviour of ODS alloys using Inconel alloy MA6000 as a model system. The paper continues in section 2.0 with a short review of the role of grain geometry in the creep behaviour of ODS alloys, and, following the experimental details in section 3.0, the results of new tensile and compressive creep tests on MA 6000 are given in section 4.0. Various models are then presented and discussed in section 5.0 where it is concluded that, for transverse loading, models based on constrained cavity growth are physically unrealistic. It is suggested that a model based on inhibited diffusional creep and cavity growth is more likely to be applicable. The paper closes with a short summary containing the main conclusions in section 6.0.

2.0 The Influence of Grain Geometry on the Creep Behaviour of ODS alloys

Grain boundaries subjected to a tensile stress at elevated temperature accumulate damage in the form of cavities which, after linking up into microcracks, result in material failure. This is the normal failure mode in creep for many polycrystalline alloys in general, but because the matrix strength of dispersion strengthened alloys is so high and the imposed operating conditions of stress and temperature are so severe, the strength differential between matrix and grain boundaries in ODS alloys is particularly marked. It is fortunate therefore that, following controlled thermo-mechanical working, ODS alloys acquire elongated grain structures which minimise the grain boundary area lying normal to a uniaxial tensile stress.

Wilcox and Clauer (3) were the first to demonstrate, in Ni-Cr-ThO_2 alloys, the importance of the grain aspect ratio (GAR) rather than the grain size per se for good high temperature strength. The effect was interpreted as being due to the reduction of grain boundary area normal to the maximum principal tensile stress and the suppression of grain boundary sliding. Of course the grain size itself should be large enough to restrict excessive creep deformation by diffusional flow.

Several workers have investigated the influence of GAR on the creep behaviour of ODS alloys. Creep data for MA 6000 reported by Cairns et al. (4) and Arzt and Singer (5) are displayed in Figure 1, which shows how the time to failure increases with GAR. Above a GAR of about 15 fracture occurs transgranularly and the material approaches its "single crystal" limit. Similar observations have been reported for bubble strengthened tungsten (8).

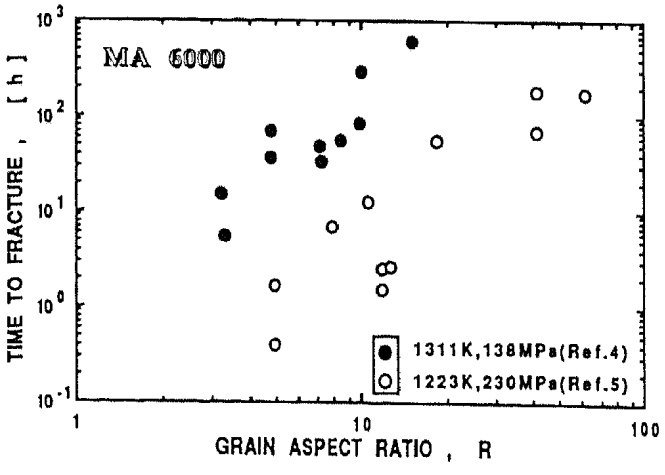

Fig.1: Creep rupture life as a function of GAR in MA 6000.

Various models have been offered as an explanation for these observations, most notably by Arzt and Singer (5), Stephens and Nix (6) and Zeizinger and Arzt (7). All models have a common feature; fracture damage accumulation on grain boundaries normal to the tensile stress is assumed to be constrained by displacements of the surrounding, undamaged, regions. In this way the geometry of the situation results in a relationship between the GAR and the creep deformation rate (or fracture time) . This is understandable since the applied stress is distributed, by an extent depending on the magnitude of the GAR, between the damaged and undamaged regions respectively. Details of the various models differ with respect to the nature of the accommodating creep mechanism. Arzt and Singer (5) attempted an explanation of their results, shown in Figure 1, by assuming cavity growth to be accommodated by grain boundary sliding of the longitudinal grain boundaries, which leads to a natural and direct linear dependence of the time to fracture on the GAR. Since cavity growth and grain boundary sliding are both linearly dependent on stress, a threshold stress for both of the diffusion - controlled processes had to be invoked in order to achieve an adequate correlation with the experimental data. It is now generally accepted, however, that grain boundary sliding alone is not possible in polycrystalline materials without accompanying grain strain accommodation (9,10), a feature that has received general confirmation in ODS alloys (7,11).

The other, more reasonable, explanation considers cavity growth to be constrained by dislocation creep which leads to strong GAR dependence on the rupture time. Models for this have been developed by Stephens and Nix (6) and Zeizinger and Arzt (7), the main aspects of which will be included in section 5.0 on modelling. Stephens and Nix (6) were able to correlate the stress dependence of the strain rate at low stress in MA 754 having intermediate and low GAR structures, where fracture occurred intergranularly, although at the lowest stresses the model consistently underestimated the creep rate. Zeizinger and Arzt (7) developed a similar model, adapted from the constrained cavity growth analysis for equiaxed grain structures given by Cocks and Ashby (12), which showed a good correlation with the results of Arzt and Singer (5).

The models developed so far have not been applied to the important situation arising in transverse loading where the grain geometry naturally results in tensile forces acting across large tracts of grain boundary area. In this case it is questionable whether a grain constraint exists at all.

3.0 Experimental Techniques

3.01 Materials

INCONEL Alloy MA 6000 bar stock with section size 60 mm x 20 mm in the fully heat treated condition (1h 1500 K, 2h 1230 K, 24h 1120 K) was used in the present study. The grain structure, consisting of highly elongated grains, is shown in Figure 2. Longitudinal grain lengths, L_1, reach upto 10 mm; the mean linear intercept length was determined as 3.7 mm. In a transverse section (Figure 3) grain dimensions are rather irregular. The mean linear intercepts of the long transverse (L_2) and short transverse (L_3) grain lengths were determined as 301 μm and 176 μm respectively. This corresponds to a GAR in the transverse direction of 1.7. The GAR in the longitudinal direction, determined from GAR= $L_1/(L_2 \cdot L_3)^{1/2}$, is 16.

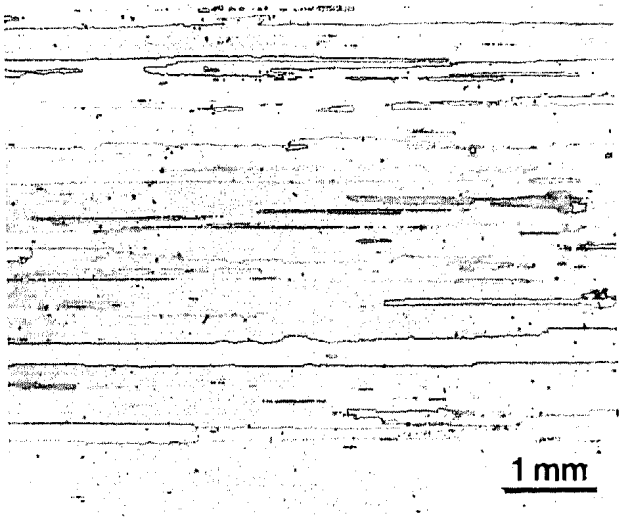

Fig.2: Longitudinal grain structure of MA 6000, GAR=16 (As-received).

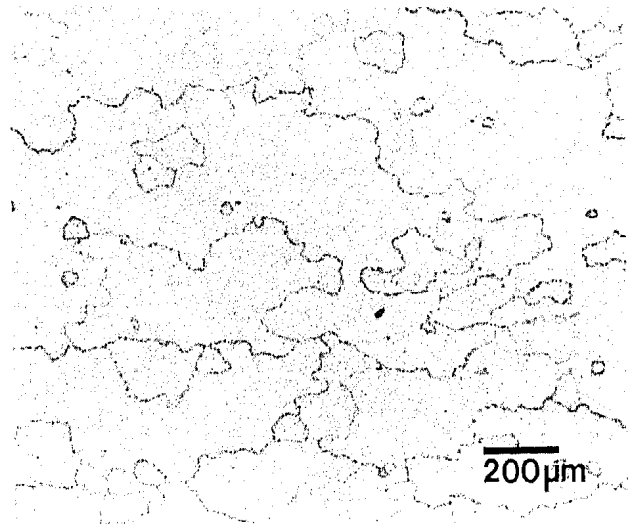

Fig.3: Transverse grain structure of MA 6000, GAR=1.7 (As-received).

In addition a 40 mm diameter bar of fine-grained material was available for producing model microstructures through secondary recrystallisation. Rods of 10 mm diameter spark machined from the bar stock were zone annealed in two stages from opposite ends of the rod under controlled conditions, which allowed grain structures to be produced approaching those of a bicrystal configuration (see section 4.0). Following zone annealing the rods were given the standard heat treatment.

3.02 Creep Testing

Tensile creep specimens with nominal dimensions 30 mm gauge length and 4 mm diameter were machined with the long transverse grain direction lying along the specimen axis. A few specimens were additionally produced from the longitudinal direction. Creep testing under constant load was conducted in an Amsler 5kN creep machine. Thermocouples attached to the specimen enabled the temperature to be controlled to within ± 2 K. Two 5 mm displacement transducers, mounted into a pair of nickel base alloy rod-in-tube extensometers, allowed for continuous displacement-time measurements to be recorded. Tests at the lowest stresses were interrupted before failure; the longest test, at 40 MPa, lasted ~ 1000h.

Compression creep tests, under constant load, were conducted in a Schenck-Trebel 100kN universal testing machine. Tests were performed in the longitudinal, long transverse and short transverse directions using cylindrical specimens 18 mm long and 9 mm diameter. A 1.5 mm displacement transducer connected between two ceramic rods, side mounted onto the specimen surface, allowed for a continuous measurement of displacement. Heating was performed by high frequency induction regulated by three thermocouples which were spot welded with equal spacing along the specimen length. At high stress creep testing was restricted to approximately 2% strain within which the steady state or minimum creep rate could be determined. At low stress a continuously decreasing strain rate was often noted. In these cases final creep rates are reported. Although, in the main, the compression creep tests were of relatively short term, a reasonable estimate of the creep rate could be achieved. All tests, in both tension and compression, were conducted at 1323 K.

4.0 Results

4.01 Tensile Creep Testing

An example creep curve for MA 6000 (65 MPa, 1323 K) tested in the long transverse direction is shown in Figure 4. Following a primary creep range the creep rate reached a steady state and terminated in a tertiary stage prior to failure. All tensile testing in the transverse direction resulted in an intergranular failure, illustrated by the SEM micrograph in Figure 5. The strains to failure were in the range 0.2 - 1.0%.

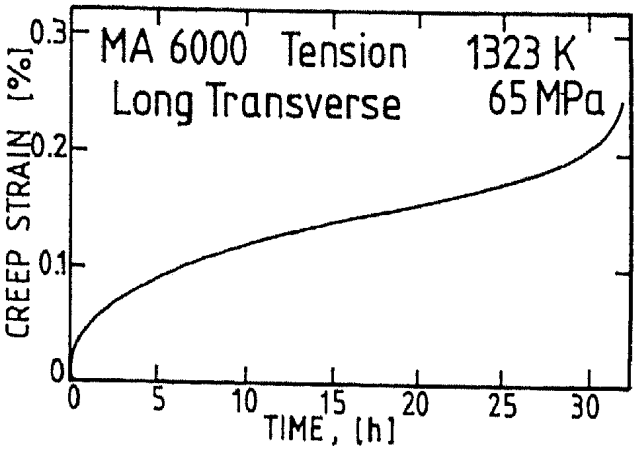

Fig.4: Example creep curve for MA 6000 under transverse loading.

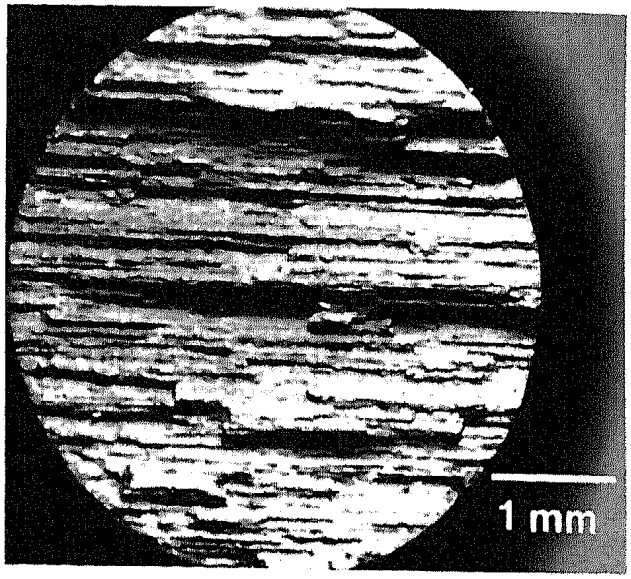

Fig.5: SEM-micrograph showing intergranular fracture in a transverse creep specimen (T=1323 K,σ=65 MPa).

All tensile creep results are plotted on double logarithmic axes in Figure 6. Although there is considerable scatter, the long transverse data can be reasonably described by a straight line of slope ~7. The longitudinal data agree well with previously published results (full line) taken from reference 13, which can be described using the following constitutive equation:

$$\dot{\varepsilon} = \dot{\varepsilon}_0 \left[\frac{\sigma}{\sigma_0}\right]^n \qquad \text{Eq.[1]}$$

with $\dot{\varepsilon}_0=10^{-11}\ s^{-1}$, $\sigma_0=116$ MPa and n=23.5.

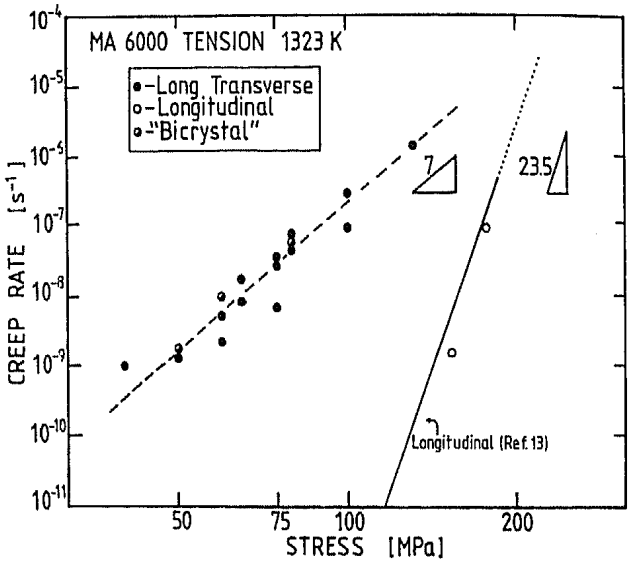

Fig.6: Tensile creep data for MA 6000 in the long transverse and the longitudinal grain direction. The "bicrystal" creep data are also shown.

The tensile creep results confirm the considerable loss in creep strength incurred under transverse loading in comparison to loading in the longitudinal grain direction. Metallographic examination of polished and etched sections taken from fractured specimens revealed profuse grain boundary cavitation lying predominantly on grain boundaries normal to the tensile stress axis (Figure 7). At positions well away from the fracture face individual, spherically shaped, cavities were observed, separated by a white etching zone devoid of γ' precipitates (Figure 8). These observations strongly suggest that diffusional cavity growth mechanisms are involved. The cavity spacing was estimated to lie between 5 and 10μm.

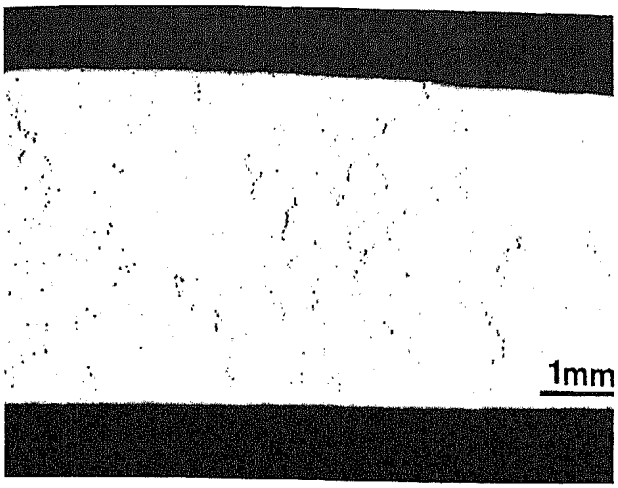

Fig.7: Profuse grain boundary cracking in MA 6000 after creep testing in the long transverse direction (T=1323K,σ=75MPa).

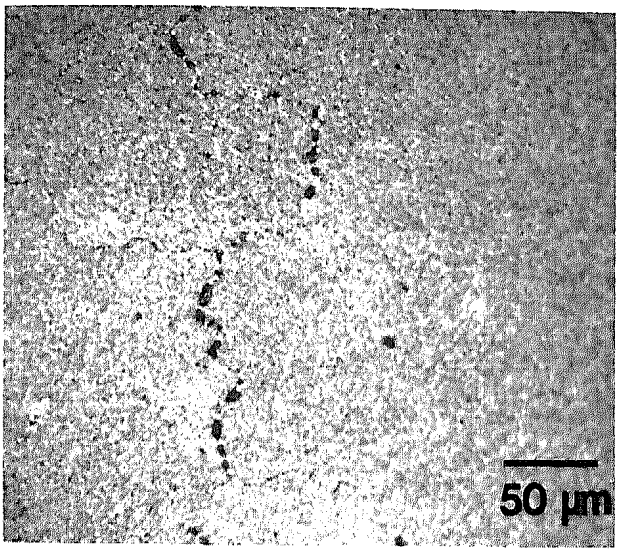

Fig.8: Creep cavities lying on grain boundaries normal to the tensile stress axis (horizontal). Note γ'-denuded zones between cavities.

4.02 Compression Creep Testing

Whereas in the longitudinal grain direction creep is similar in tension and compression (Figure 9), transverse creep in tension is considerably impaired in comparison to creep in compression (Figure 10). Surprisingly, a comparison between the compressive creep behaviour in the longitudinal and transverse directions also revealed significant differences; creep rates are enhanced in the transverse directions (Figure 11). Creep rates in the short transverse direction were found to be, especially at high stress, somewhat faster than in the long transverse direction. The compressive creep data are plotted on double logarithmic axes in Figure 12, which clearly illustrates the enhancement in the transverse creep rates at low stress in comparison to those in the longitudinal direction.

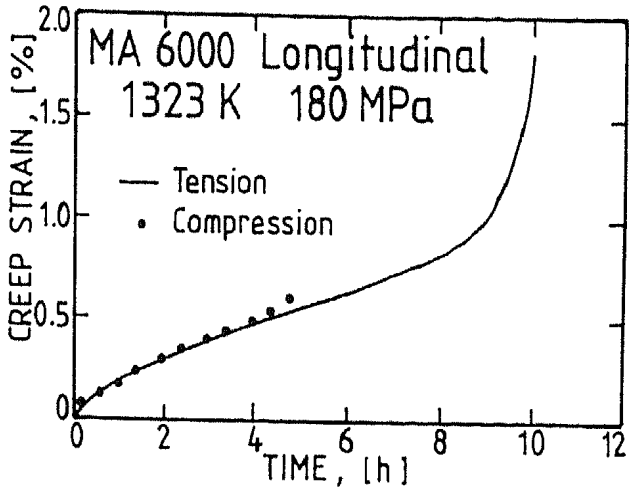

Fig.9: Comparison between tensile and compressive creep in the longitudinal direction.

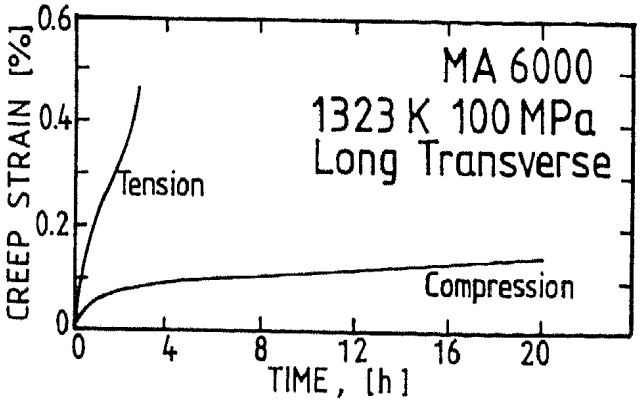

Fig.10: Comparison between tensile and compressive creep in the long transverse direction.

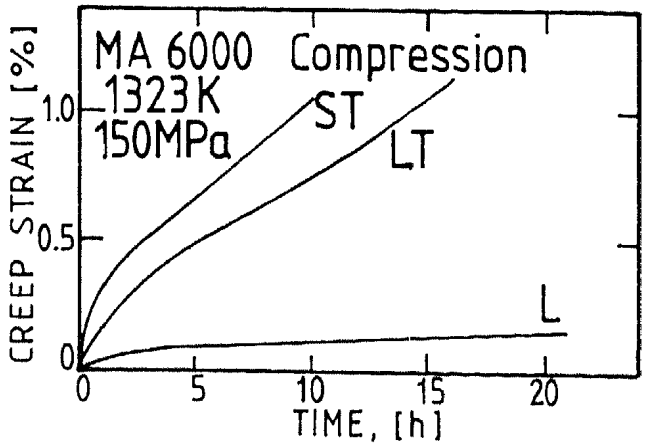

Fig.11: Comparison between compressive creep in the longitudinal, long transverse and short transverse directions.

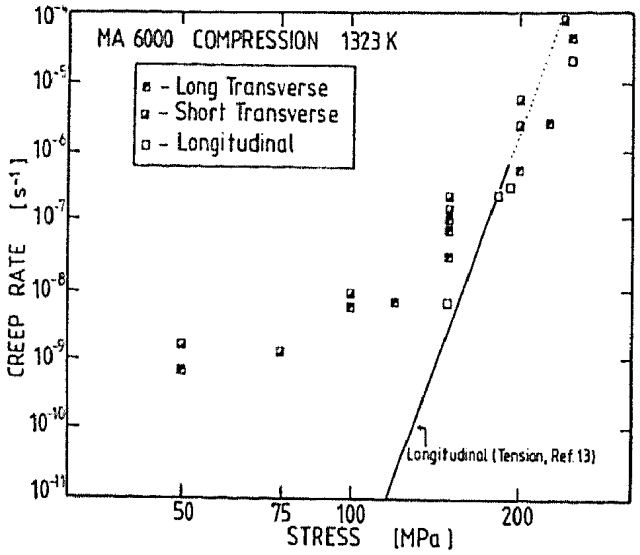

Fig.12: Compressive creep data for MA 6000 in the transverse directions (longitudinal creep data are also plotted for comparison).

Metallographic examination of samples tested in the transverse direction under compressive loading revealed white etching bands adjacent to grain boundaries oriented parallel to the compression stress axis (Figure 13), which have previously been confirmed as devoid of γ' (14). This feature is strong evidence for the operation of a stress directed diffusional creep mechanism. Furthermore, closer observation revealed local changes in the carbide particle distribution (Figure 14); within the γ'-depleted zones a population of ~ 1 μm sized carbide particles, identified as being W and Mo rich, was observed. Grain boundaries perpendicular to the compression stress axis were carbide free. Moreover, these local changes in microstructure were neither observed in as-received nor in merely stress-free annealed material. Attempts have been made, using EDAX in SEM, to determine the yttrium distribution across the γ'- denuded zones. A tendency was found for a reduced Y concentration adjacent to the grain boundary, but the low resolution of the technique did not allow for a firm conclusion to be reached. We await further results from a microprobe analysis.

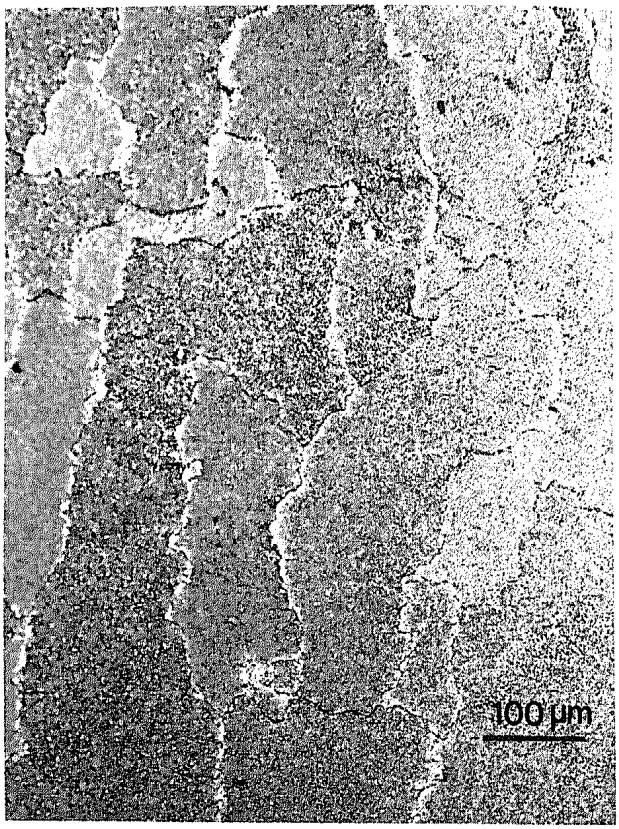

Fig.13: Microstructure following compressive creep in the long transverse direction. Note γ'-depleted zones adjacent to grain boundaries oriented parallel to the compressive stress axis (vertical). T=1323K,σ=120 MPa.

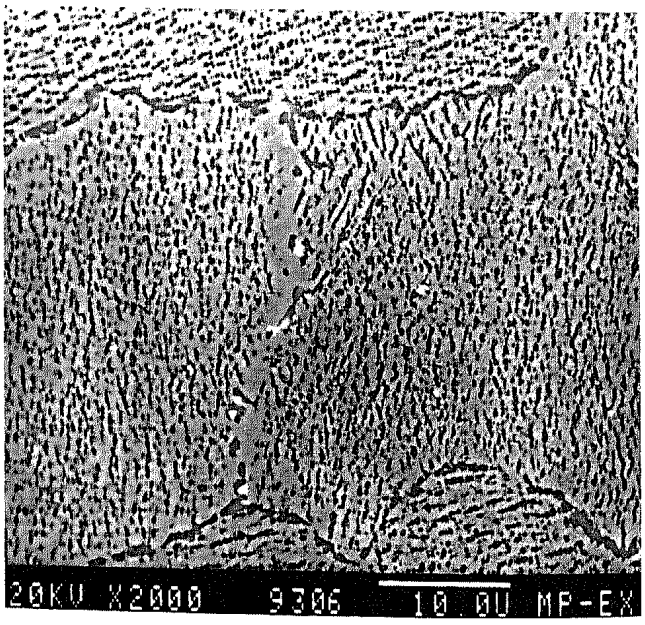

Fig.14: γ'-denuded zones after compressive creep in the long transverse direction. Note carbide particles within the zone and absence of carbides on the other grain boundaries (stress axis vertical, T=1323K,σ=120 MPa).

4.03 "Bicrystal" Creep Testing

As mentioned in section 3.0 model microstructures having a bicrystal configuration have been produced by sequential zone annealing from opposite ends of specimen rods. The grain structure is depicted in Figure 15 showing how the highly elongated grains meet at a common junction. A few tensile creep tests have been performed on these "bicrystals"; example creep curves, compared with those for the long transverse direction are shown in Figure 16. The times to fracture for the "bicrystal" tests were consistently less than the transverse tests, but the creep rates (also plotted in Figure 6) were, within experimental scatter, surprisingly equivalent. Further reference to these results will be made in the next section.

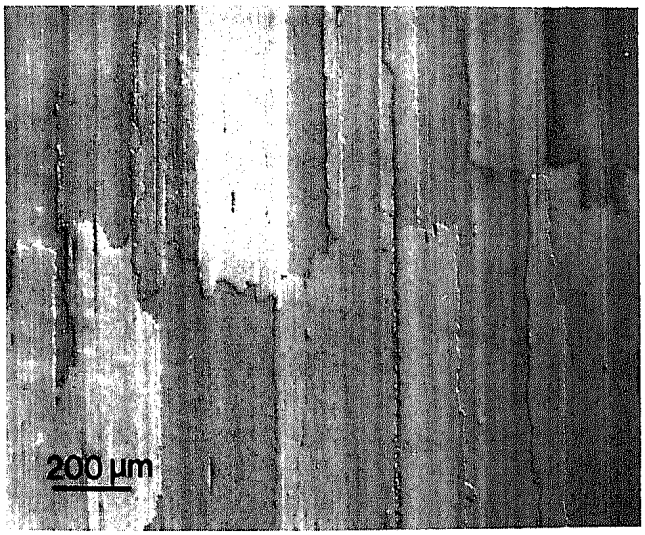

Fig.15: Model "bicrystal" grain structure produced by controlled secondary recrystallisation of fine-grained material.

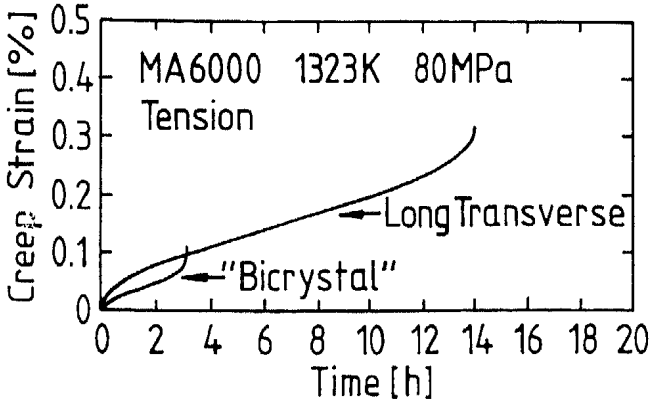

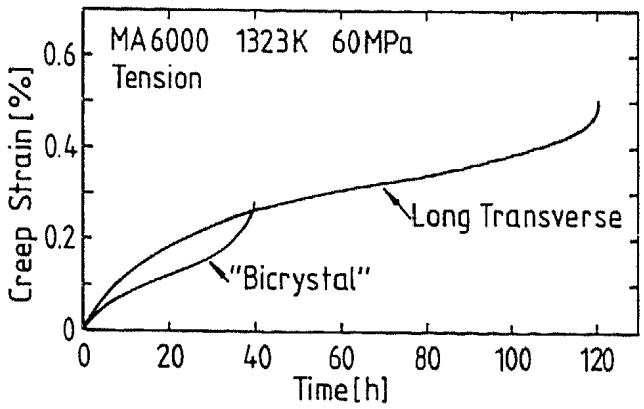

Fig.16: Example creep curves of the "bicrystal" specimens in comparison to the long transverse direction.

5.0 Discussion and Modelling of the Transverse Creep Behaviour of ODS Alloys

In this section an attempt is made to model the transverse creep behaviour of MA 6000: further details will be published shortly (15).

In view of the success of constrained cavity growth models in describing the longitudinal creep behaviour of ODS alloys as a function of GAR (6,7), it is considered instructive, as a first step, to assess the appropriateness of this modelling approach to the transverse creep behaviour. The main features of these models are contained within the following set of assumptions:

- cavities nucleate on grain boundaries normal to the tensile stress axis and grow by grain boundary diffusion
- void growth is accommodated by dislocation creep in the surrounding, undamaged, grains
- in order to maintain material compatibility the displacement rates in the damaged and undamaged regions are equal.

From these assumptions the following relationship results between the applied stress, σ_∞, and the macroscopic creep rate, $\dot{\varepsilon}_\infty$, including the influence of the grain aspect ratio, R:

$$\frac{\sigma_\infty}{\sigma_0} = \frac{\dot{\varepsilon}_\infty}{A \cdot R} + \frac{R-1}{R}\left[\frac{\dot{\varepsilon}_\infty}{\dot{\varepsilon}_0}\right]^{1/n} \qquad \text{Eq.[2]}$$

where A is a material constant taken from Cocks and Ashby (12),

$$A = \frac{4D_b\omega\ \Omega\ \sigma_0}{kT\ L\ \lambda^2\ ln(1/f)} \qquad \text{Eq.[3]}$$

$D_b\omega$ is the grain boundary diffusion coefficient times the grain boundary width, f is the cavitated area fraction, $(r/\lambda)^2$, r is the void radius and 2λ is the cavity spacing. The other symbols have either been given previously or take their usual meanings.

Equation [2] has been evaluated and is plotted, together with the experimental tensile creep results in Figure 17, for both R=1.5, 2λ=5μm and R=2.0, 2λ=10μm, which are reasonable limits for the most sensitive parameters entering into Eq.[2]. L is set equal to the long transverse grain length (L_2) and values for the other parameters are taken from Frost and Ashby (16). The plot shows how the model calculations bound the bulk of the data, but the stress sensitivity of the creep rate is overestimated. The extreme sensitivity of the predicted creep rate to the grain aspect ratio at low GAR is obviously unrealistic. For example at a stress of 50 MPa a small increase in GAR from 1.5 to 2.0 is predicted to raise the strain rate by over four orders of magnitude. The reason lies in the assumption that void growth occurs by classical diffusional mechanisms such that for R=1, which represents a situation where no matrix creep constraint acts (fully cavitated equiaxed polycrystal or bicrystal), a linear stress dependency of the creep rate is predicted. Further model calculations are illustrated in Figure 18 showing how, at low GAR, the stress-creep rate curve changes dramatically on varying GAR by a small, practically insignificant, amount.

The weakness of the constrained cavity growth model lies in the acceptance of the equations for the classical diffusional mechanisms. The micro-structural evidence presented in section 4.0 showed clearly that diffusional creep processes do indeed make a significant contribution to the overall creep behaviour in MA 6000. However, it is unlikely that in these dispersion hardened materials diffusional creep rigidly obeys the classical diffusional creep theories. One of the main assumptions of the above model, therefore, cannot be accepted without criticism. Moreover, it is questionable whether the assumption regarding cavity growth constrained by matrix deformation is reasonable for loading in the transverse direction, in which the highly elongated grains extend across virtually the total creep specimen diameter, as already illustrated in Figure 5. Additionally, the model explicitly predicts a linear stress dependence of the creep rate for testing in the short transverse direction. Creep results, however, have shown that the stress exponent, for the time to fracture at least, remains well in excess of 1 (17). Although some of the problems may be caused by the assumption of an idealised grain geometry used in the modelling, we believe there is little scope for making any significant improvements in the predictions of the constrained cavity growth model when applied to low GAR structures.

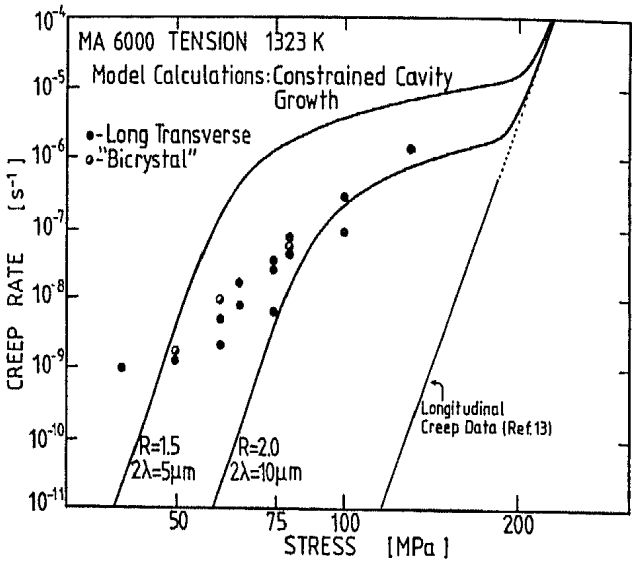

Fig.17: Comparison between model calculations for constrained cavity growth and the transverse tensile creep data.

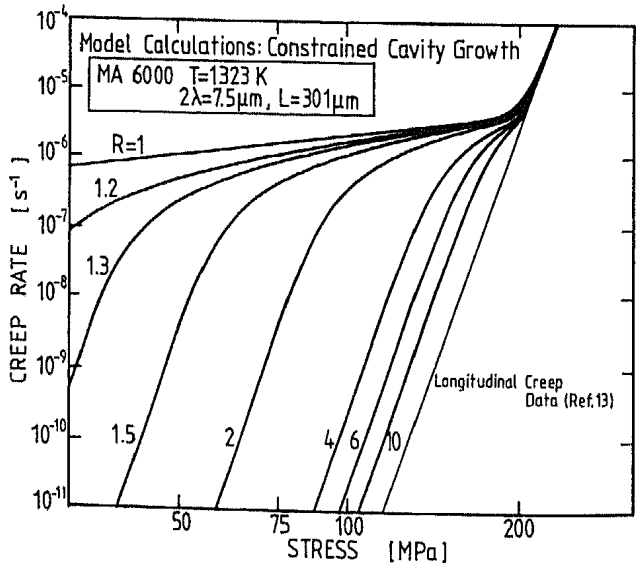

Fig.18: Constrained cavity growth model calculations. Note the extreme sensitivity of the stress-strain rate curve to the GAR at low GAR.

These reasons led to the motivation for conducting the "bicrystal" creep tests, since these would be, in principle, the optimum solution to confirm the applicability of classical diffusional cavity growth theories. The grain structure depicted in Figure 15 reveals that the grains are slightly interlocked, but because of this small degree of waviness we believe such a structure offers negligible matrix constraint to any cavity growth. Hence, the similar strength of the long transverse and the "bicrystal" creep specimens, as described in section 4.0, sheds doubt on the validity of the constrained cavity growth model in the present investigation. They further bring into question the appropriateness of using classical diffusional creep theories alone (see below).

In the following a new model is presented based on interface reaction controlled diffusional creep. In tension, at low stress levels, the creep rates predicted by classical diffusional cavity growth thoery are far greater than the measured creep rates (represented by the R=1 line in Fig.18), and the predicted linear stress sensitivity of the creep rate is not observed. Under compressive loading cavity growth is suppressed, but diffusional creep deformation is not, even though the grains are highly elongated. The reason is (18,19) that, under transverse loading, the vacancy flux adopts a two dimensional form resulting in a creep rate dependent only on the transverse grain dimensions and independent of the long grain length. When lattice diffusion is rate controlling the constitutive equation for transverse Nabarro-Herring creep in an elongated grain structure becomes (18,19):

$$\dot{\varepsilon} = \frac{12 D_v \Omega}{kT} \cdot \frac{\sigma}{L_2^2 + L_3^2} \qquad \text{Eq.[4]}$$

It is well known that in order for diffusional creep processes to continue in an uninhibited manner, the supply of vacancies from the grain boundary must be maintained at the required level as governed by the applied stress. If the creation or annihilation of vacancies is in any way impeded, then the diffusional creep rate will become progressively dependent on the kinetics of the vacancy creation process. It is generally considered that vacancies are created and destroyed via the climb of grain boundary dislocations (20,21), which, therefore, will have to by-pass the dispersoids lying in the grain boundary plane in order to act as efficient sources and sinks for vacancies (22).

We suggest that grain boundary dislocations overcome dispersoids in a similar manner to the way in which matrix dislocations by-pass inert dispersoids in ODS alloys (1,2); dislocations will be strongly pinned at the particle interface as a consequence of an attractive interaction, and thermal activation will be necessary for dislocation detachment. If the stress is too low or the thermal activation is insufficient, then creep due to stress directed diffusion of point defects stops. We realise there is virtually no evidence in the literature for such a mechanism and experimental verification may prove extremely difficult because of the problems involved in imaging grain boundary dislocation - particle interactions in TEM: one report, however, supports this hypothesis (23). In addition, a theoretical analysis has so far not been attempted, but, in analogy with matrix creep behaviour in ODS alloys, we may estimate what sort of features a constitutive equation based on the thermally activated detachment of grain boundary dislocations from inert dispersoids may have. These may include a relatively high stress sensitivity of the dislocation mobility over a large stress range, activation energies for creep far greater than that for the simple diffusional process, and pseudo-threshold stress behaviour.

In general, diffusional cavity growth and diffusional creep superimpose on power law matrix dislocation creep. Therefore three independent strain producing components can be identified:

1) Interface reaction controlled diffusional cavity growth,

$$\dot{\varepsilon}_1 = \dot{\varepsilon}_v / [1 + (\dot{\varepsilon}_v / \dot{\varepsilon}_m)] \qquad \text{Eq.[5]}$$

where,

$$\dot{\varepsilon}_v = \frac{B D_b \omega \Omega}{kT} \cdot \frac{\sigma}{\lambda^2 L_2} \qquad \text{Eq.[6]}$$

and $\dot{\varepsilon}_m$ is discussed below.

2) Interface reaction controlled diffusional creep deformation,

$$\dot{\varepsilon}_2 = \dot{\varepsilon}_v / [1 + (\dot{\varepsilon}_v / \dot{\varepsilon}_m)] \qquad \text{Eq.[7]}$$

where in this case,

$$\dot{\varepsilon}_v = \frac{C D_v \Omega}{kT} \cdot \frac{\sigma}{L_2^2 + L_3^2} \qquad \text{Eq.[8]}$$

3) Power law creep,

$$\dot{\varepsilon}_3 = \dot{\varepsilon}_0 \left[\frac{\sigma}{\sigma_0} \right]^n \qquad \text{Eq.[9]}$$

Under tensile loading in the transverse direction the creep rate is given by,

$$\dot{\varepsilon}_T = \dot{\varepsilon}_1 + \dot{\varepsilon}_2 + \dot{\varepsilon}_3$$

whereas under compressive loading, where cavity growth does not occur, the creep rate is,

$$\dot{\varepsilon}_C = \dot{\varepsilon}_2 + \dot{\varepsilon}_3$$

In order to proceed further we need a constitutive equation for $\dot{\varepsilon}_m$, which describes the interface reaction. Lacking a detailed thoery for the grain boundary dislocation - dispersoid interaction, we choose to adopt, for the present time at least, an expression for $\dot{\varepsilon}_m$ that simply fits the bulk of the tensile creep data in a reasonable way. We find that a simple power law form for $\dot{\varepsilon}_m$ suffices as follows:

$$\dot{\varepsilon}_m = \dot{\varepsilon}_{m_0} \left[\frac{\sigma}{\sigma_m}\right]^m \qquad \text{Eq.[10]}$$

with $\dot{\varepsilon}_{m_0}=10^{-10}\ s^{-1}$, $\sigma_m=40$ MPa and m=10.

Using the above relationship, the appropriate combinations of the creep processes 1, 2 and 3 for tensile and compressive loading respectively have been evaluated, and are plotted, together with all the creep data, in Figure 19. The individual uninhibited diffusional creep rates, and the creep rate due to power law creep are also displayed in Figure 19 as dashed lines. Although we have purposely selected a constitutive equation for $\dot{\varepsilon}_m$, we believe the present approach, summarised by Figure 19, is encouraging in two respects:

- firstly, the theoretical creep rates due to both cavity growth and Nabarro-Herring creep predict very well the respective limits of the tensile and compressive creep rate data,
- secondly, through the choice of a single, relatively simple, relationship for $\dot{\varepsilon}_m$, both the tensile and the compressive creep data can be interpreted in a consistent manner.

The assumption that diffusional creep mechanisms in MA 6000 are controlled by an interface reaction is the crucial step in the present modelling approach. In itself this is not unrealistic, but verification of the validity of the constitutive equation for the interface reaction and the details of the mechanism will require further work. An interface reaction process based on a dispersoid - grain boundary dislocation interaction is certainly plausible. It will be necessary to conduct detailed TEM - investigations in order to ascertain whether such a mechanism indeed occurs in these alloys. In addition a theoretical analysis will be required to support these considerations.

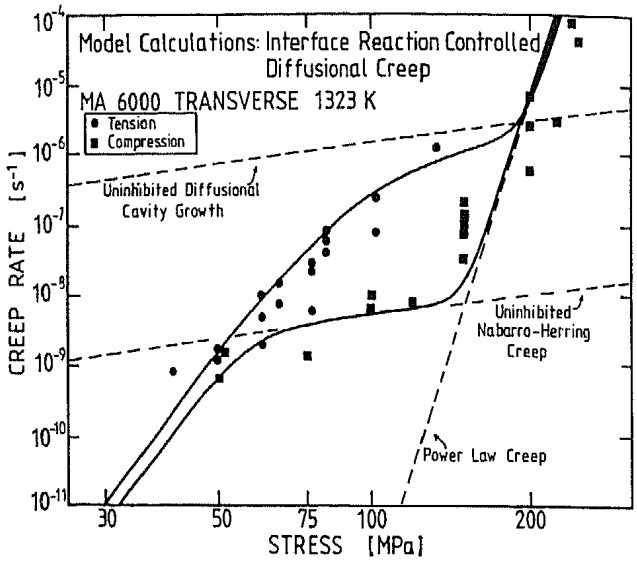

Fig.19: Comparison between model calulations for interface reaction controlled diffusional cavity growth and creep deformation and the transverse tensile and compressive creep data.

It seems clear that the transverse creep behaviour of coarse-grained ODS alloys will, in general, always be inferior to that of the longitudinal direction. Significant improvements in strength would be possible if cavity nucleation could be suppressed. Under the present circumstances this stage of the fracture process occurs relatively easy, and coarse oxide particles are the likely sites for void nucleation. Increased creep strength should be possible through a reduction in the population of the coarse oxide inclusions, which are often present in ODS alloys as stringers located on the longitudinal grain boundaries. Under transverse loading their effect is therefore extremely detrimental.

6.0 Summary and Conlusions

Tensile creep tests on MA 6000 indicate that models based on matrix creep constrained cavity growth are inappropriate for creep in the transverse grain direction. A model based on interface reaction controlled diffusional cavity growth is suggested to be more realistic. Under compression diffusional creep deformation is important which can also be included within the present model framework. Although many details of the micromechanisms involved remain unclear, the present approach can provide a basis for a better understanding of the transverse creep behaviour

of ODS alloys. It is suggested that only by reducing the density of the coarse oxide inclusions can significant improvements in the transverse creep strength be acheived.

Acknowledgements

We are especially grateful to Mr K. Lempenauer for producing the "bicrystal" specimens. Particular thanks go to Mr D. Lang, Mrs S. Miller and Mrs C. Elzey for assistance with the creep testing and metallography. We wish to acknowledge the financial support of the Bundesministerium für Forschung und Technologie in the FRG under project number 03 M0013.

REFERENCES

[1] Arzt, E. (1988) in "New Materials by Mechanical Alloying Techniques", p185 Eds. E. Arzt and L. Schultz, DGM, Oberusel, FRG.

[2] a) Rösler, J. and Arzt, E. Acta Metall., in press.
b) Rösler, J. and Arzt, E. (1988) Acta Metall., 36, 1043.
c) Arzt, E. and Rösler, R. (1988) Acta Metall.,36, 1053.

[3] Wilcox, B.A. and Clauer, A.H. (1972) Acta Metall., 20, 743.

[4] Cairns, R.L., Curwick, L.R. and Benjamin, J.S. (1975) Metall. Trans., 6A, 179.

[5] Arzt, E. and Singer, R.F. (1984) in "Superalloys 84", p367, Eds. M. Gell et al. TMS-AIME, Warrendale.

[6] Stephens, J.J. and Nix, W.D. (1986) Metall. Trans. 17A, 281.

[7] Zeizinger, H. and Arzt, E. (1988) Z. Metall., 79, 774.

[8] Wright, P.K. (1978) Metall. Trans., 9A, 955.

[9] Raj, R. and Ghosh, A.K. (1981) Metall. Trans., 12A, 1291.

[10] Anderson, P.M. and Rice, J.R. (1985) Acta Metall., 33, 409.

[11] Stephens, J.J. and Nix, W.D. (1985) Metall. Trans., 16A, 1307.

[12] Cocks, A.C.F. and Ashby, M.F. (1982) Prog. Mat. Sci., 27, 189.

[13] Guttman, V. (1988) in COST 501 Summary Report by E. Arzt and R. Timmins.

[14] Timmins, R. and Arzt, E. (1988) Scripta Metall., 22, 1353.

[15] Timmins, R. and Arzt, E. (1990) to be published.

[16] Frost, H.J. and Ashby, M.F. (1982) "Deformation-Mechanism Maps", Pergamon Press, Oxford.

[17] Nazmy, M., Staubli, M. and Ebeling, W. (1987) Mat. Technik, 15, 9.

[18] Nix, W.D. (1981) Metals Forum, 4, 38.

[19] Greenwood, G.W. (1985) Phil. Mag., 51, 537.

[21] Balluffi, R.W. (1980) in "Grain Boundary Sructure and Kinetics", Ed. R.W. Balluffi, ASM, Metals Park, Ohio.

[22] Arzt, E., Ashby, M.F. and Verrall, R.A. (1983) Acta Metall., 31, 1977.

[23] Dunlop, G.L., Nilsson, J.-O. and Howell, R.R. (1979) J. Microscopy, 116, 115.